CFD modelling and experimental analysis of aromatic amine extraction in a flat sheet supported liquid membrane contactor

Gilles Van Eygen[a,b,c,*], Emma Lodewijckx[a], Sean Van Gestel[a], Nilay Baylan[a,d], Anita Buekenhoudt[c], João A.P. Coutinho[e], Bart Van der Bruggen[a], Patricia Luis[b,f]

a Process Engineering for Sustainable Systems (ProcESS), KU Leuven, Celestijnenlaan 200f, 3001 Leuven (Belgium)

b Materials & Process Engineering (IMAP), UCLouvain, Place Sainte Barbe 2, B-1348 Louvain-la-Neuve (Belgium)

c Unit Separation and Conversion Technology, Vlaamse Instelling voor Technologisch Onderzoek (VITO NV), Boeretang 200, 2400 Mol (Belgium)

d Department of Chemical Engineering, Istanbul University-Cerrahpaşa, Avcılar, 34320, Istanbul, Turkey

e CICECO-Aveiro Institute of Materials, Chemistry Department, University of Aveiro, 3810-193 Aveiro, Portugal

f Research & Innovation Centre for Process Engineering (ReCIPE), Place Sainte Barbe 2, bte L5.02.02, B-1348 Louvain-la-Neuve (Belgium), Tel: +32 (0)10 47 25 87 - Fax: +32(0)10 47 40 28

* Corresponding author. Tel: +32-14-336-907. E-mail: gilles.vaneygen@vito.be (Gilles Van Eygen)

Abstract

Supported liquid membranes (SLMs) using ionic liquids are effective for the extraction of aromatic amines. This experimental study employed a flat sheet SLM contactor with the ionic liquid trihexyltetradecylphosphonium bis(trifluoromethylsulfonyl)imide ($[P_{6,6,6,14}][N(Tf)_2]$) as the solvent to investigate the separation of α-methylbenzylamine (MBA) and 1-methyl-3-phenylpropylamine (MPPA) from isopropyl amine (IPA). A detailed process study was conducted to examine the effects of flow rate (5 – 10 L/h), feed concentration (0.5 – 2.5 g/L), and feed pH (9 – 11) on extraction performance. Under standard experimental conditions (10 L/h, 1.0 g/L, pH 10), MBA and MPPA demonstrated high solute fluxes of 2.39 and 5.47 g/(m²h), respectively, compared with IPA, which had a solute flux of 0.84 g/(m²h). However, after 24 hours, the recoveries were relatively low, at 17.9% for MBA, 32.6% for MPPA, and 5.2% for IPA. No significant velocity dependency was observed, with slight variations attributed to minor pH changes, while a linear flux increase was noted for higher feed concentrations. The feed pH had a significant impact on the extraction performance, with higher pH levels resulting in increased solute fluxes and recoveries. To complement the experimental results, computational fluid dynamics (CFD) simulations were employed using COMSOL Multiphysics 5.1. The model demonstrated satisfactory agreement across various conditions, but underestimated fluxes and recoveries at higher pH values. Consequently, a new mass transfer mechanism was proposed to explain the variations observed in the experimental results.

Keywords — Ionic liquids, supported liquid membranes, extraction, computational fluid dynamics.

1. Introduction

Chiral amines are important intermediates in the production of a large variety of bioactive compounds, used in the agrochemical, pharmaceutical, and related industries [1,2]. While various methods are available for synthesizing these compounds, the direct asymmetric synthesis method using transaminase enzymes is the preferred pathway, due to its potential for achieving a theoretical yield of 100% [3]. However, a major challenge of this enzymatic reaction is its low equilibrium constant. To address this, *in situ* product removal through liquid-liquid extraction can be employed to shift the equilibrium toward the desired product. Although liquid-liquid extraction is a common technique for the recovery of chiral amines, the biocatalyst stability can be compromised upon contact with certain extractants [4,5]. Additionally, industrial-scale liquid-liquid extraction often requires large volumes of toxic solvents to be effective [6].

To minimize the use of toxic solvents, researchers have explored alternative solvents such as ionic liquids, deep eutectic solvents, and supramolecular liquids [7]. However, liquid-liquid extraction techniques still require direct contact between the solvent and the enzyme. Membrane extraction (ME) offers an alternative by physically separating the feed and extractant phases with a membrane, preventing this contact [4,5]. ME also provides advantages such as high selectivity, low energy consumption, and operational simplicity, though its stability can be lower in certain cases [8]. ME has already been investigated for the extraction and recovery of metal ions, organics, and pharmaceuticals, including chiral amines [9–11]. In a study by Rehn et al. [12], the chiral amine α-methylbenzylamine was extracted from a reaction broth using a hollow fibre module and undecane as the selective extractant. Moreover, alternative solvents such as ionic liquids and deep eutectic solvents can be used in combination with ME [13–16]. For example, Zurob et al. [17] employed an asymmetric ionogel-based membrane for the separation of succinic acid from fermentation broths.

Nevertheless, the overall ME performance can be affected by various process conditions, which complicates industrialisation of the process. For example, the pH conditions of the reaction can alter the separation performance, as protonation control of the product amine can lead to better separation from the (remaining) substrate

ketone [4,5,18]. To address possible process variations, computational fluid dynamics (CFD) can be used for optimisation purposes. In the last 20 years, CFD had an increase in popularity as it allows the quick testing of various processes using simulations without the need for experiments. A CFD model can provide an initial approximation, which is often sufficient for subsequent process design. An experimental validation of the results is still necessary since the models are not yet capable of fully representing reality [20–24]. In the membrane extraction field, CFD modelling has gathered momentum, as many researchers have been using simulations for process analysis [8]. Generally, single or multi-hollow fibre modules have been explored for the extraction of a variety of compounds, such as organics [25,26], metal ions [27,28], and pharmaceuticals [29,30].

This work aims to experimentally study the separation of the aromatic amines α-methylbenzylamine (MBA) and 1-methyl-3-phenylpropylamine (MPPA) from isopropyl amine (IPA) in an alkaline feed buffer using the ionic liquid $[P_{6,6,6,14}][N(Tf)_2]$ as the extractant in a flat sheet supported liquid membrane (SLM) system operated in recycle mode. The effects of various process conditions — such as flow rate, feed concentration, and buffer pH — were systematically investigated. Last, a new mass transfer mechanism was proposed based on the CFD simulations.

2. Experimental

2.1 Materials

The amines used in this work were isopropyl amine (IPA, ≥ 99.5%, Sigma-Aldrich), 1-methyl-3-phenylpropylamine (MPPA, 98%, Sigma-Aldrich) and α-methylbenzylamine (MBA, 99.0%, Fluorochem). The alkaline feed buffers used Na_2CO_3 (≥ 99.5%, Honeywell Fluka) and $NaHCO_3$ (≥ 99.7%, Sigma-Aldrich), while the acidic strip buffer used NaH_2PO_4 (≥ 99.0%, Sigma-Aldrich) and H_3PO_4 (85%, Carlo Erba Reagents). Trihexyltetradecylphosphonium bis(trifluoromethylsulfonyl)imide or $[P_{6,6,6,14}][N(Tf)_2]$ (> 98%, Iolitec GmbH) was used as the extractant. All chemicals were used without further purification. Donaldson kindly provided the 50 nm PTFE membranes (#1325) for ME testing and the 100 nm PTFE membranes with PP support (#6501) used as a nonwoven support for membrane impregnation.

2.2 Membrane extraction experiments

The alkaline feed and acidic strip buffer were prepared as given in Table S1. The different amines – MBA, MPPA, and IPA – were subsequently introduced in the feed buffer. Vacuum impregnation was used to wet the PTFE support material with the ionic liquid extractant. After aspiration, the ionic liquid was pipetted onto the membrane surface. The impregnation process lasted for 45 minutes, after which any residual liquid was wiped off the membrane surface with a paper tissue. The ionic liquid uptake was determined by weighing the membrane before and after impregnation. The used experimental setup has already been described in previous works [13,14,31]. The feed and strip buffer (250 mL each) were circulated counter-currently using two magnetically driven gear pumps. All membrane extraction experiments were performed at least in twofold and ran at a temperature of 30 ± 2 °C. The following process conditions were varied within the specified ranges: flow rate (5, 7.5, and 10 L/h), feed concentration (0.5, 1, and 2.5 g/L), and feed pH (9.0, 9.5, 10.0, 10.5, and 11.0).

2.3 Analytical methods

The feed and strip buffer were sampled (1 mL) at the start of the experiment and after 1, 3, 6, and 24 hours. The MBA and MPPA concentration were determined using HPLC-UVVIS analysis (Schimadzu Prominence-I LC-2030C 3D) using gradient elution with acetonitrile and an 0.1 v% H_3PO_4 solution as the mobile phases. The IPA concentration was determined by headspace GC-FID analysis (Autosystem XL, PerkinElmer) with helium as the mobile phase and an Rtx-5 Amine (30 m, 0.25 mm, 0.50 µm). To allow IPA volatilization, 200 µL of a 25% NaOH solution were added to the GC samples. The solute flux J_i^{exp} of amine i through the membrane phase was calculated as follows:

$$J_i^{\mathrm{exp}} = -\frac{\Delta C}{\Delta t}\frac{V}{A_{\mathrm{eff}}} \tag{1}$$

where ΔC [g/L] is the concentration difference over the time interval Δt [h], V [L] the buffer volume, and A_{eff} [m²] the effective membrane area. The solute recovery R_i^{exp} of amine i was calculated as follows:

$$R_i^{\mathrm{exp}} = \frac{C_{\mathrm{f}}^{t=0} - C_{\mathrm{f}}^{t=24\mathrm{h}}}{C_{\mathrm{f}}^{t=0}} \cdot 100 \tag{2}$$

where C_{f}^{t} [g/L] is the feed concentration at time t. The solvent usage is detailed in Section S2.

2.4 CFD simulations

A computational fluid dynamics (CFD) model was created in COMSOL Multiphysics 5.1 to simulate the amine extraction. The simulated flat sheet module is shown in Figure 1 and consisted of two mirrored spiral channels in between which a membrane of 180 µm was placed. A distinction was made between three domains, namely the alkaline and acidic buffer domain, and the membrane domain. Each buffer domain consisted of one spiral module with connecting tubes in which the buffer solution flows. The membrane domain consisted of the 180 µm spiral-shaped membrane in between these buffer domains. The specifications of the flat sheet module building in Solid Edge are given in Section S3.1.

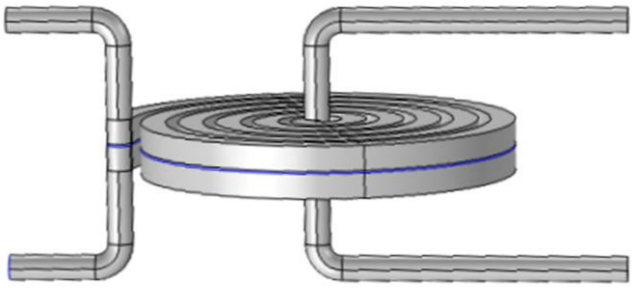

Figure 1. Spiral flat sheet module created in COMSOL.

The CFD model should be robust within broad ranges of parameter variations to guarantee its usability. To allow for the simulation of the above-mentioned phenomena, a combination of multiple physics was used. Generally, a semi-complex physics is used as the basis on which simpler physics are stacked. In this work, a multi-physics model was chosen over various single physics models, due to the limitations or complexities of those models. All assumptions and boundary conditions applied in the final model are described in Section S3. A short robustness study was conducted to assess the model's stability against variations in mesh size and boundary conditions (see Section S5). The conditions of the standard CFD simulation are detailed in Table 1.

Table 1. Parameter values for the CFD simulation at standard conditions.

	Parameter	Value	Unit
Process	Flow rate	10	L/h
	Temperature	30	°C
	Initial feed concentration	1	g/L
	Mode of operation	Counter-current	-
Buffer	Density	997	kg/m²
	Viscosity	0.7978	mPa s
	Feed pH	10	-
	Strip pH	3	-
	Buffer capacity	0.2	M
(Liquid) membrane	Density	1067.9	kg/m³
	Viscosity	297.5	mPa s

Porosity	0.67	-
Thickness	180	µm
Darcy's permeability	0.06326	D
Diffusivity	$2.5 \cdot 10^{-10}$	m²/s

Model validation was conducted by calculating the Root Mean Squared Error (RMSE) for the solute flux and recovery across all conditions and for each solute. The RMSE values were used to quantify the differences between the simulated and experimental results, providing a measure of the model's predictive accuracy. The RMSE was calculated as follows:

$$\mathrm{RMSE} = \sqrt{\frac{1}{n}\sum_{i=1}^{n}\left(x_i^{\mathrm{exp}} - x_i^{\mathrm{sim}}\right)^2} \quad (3)$$

in which n denotes the sample size, x_i^{exp} the experimentally observed value at point i, and x_i^{sim} the simulated value at point i.

2.4 COSMO-RS simulations

First, quantum calculations were performed using the TmoleX software package with density functional theory (DFT) and a resolution identity (RI) approximation. Vibrational frequency calculations were conducted to determine the electronic energy minimum. The optimised geometries of the amines, and the cation and anion under consideration were obtained using the triple zeta valence polarised basis set (def-TZVP), the Becke-Perdew (BP-86) functional, and the COSMO solvation model. These geometries were saved as COSMO files. Second, vibrational frequency calculations were carried out to confirm the presence of an optimised energy state. Third, the generated COSMO files were used as input in COSMOtherm to predict the amine diffusivities in the ionic liquid [14,32–34].

3. Results and discussion

3.1 Effect of flow conditions and membrane properties

Figure 2 displays the general velocity profile in the module. Herein, the feed side is placed on top with the inlet on the left-hand side, while the strip side is placed on the bottom with its inlet on the right-hand side. The Reynolds number can be calculated as:

$$Re = \frac{\rho u D_{\mathrm{h}}}{\eta} \tag{4}$$

with ρ the density, η the viscosity, u the crossflow velocity, and $D_{\mathrm{h}} = 4\,A_{\mathrm{fluid}}/P_{\mathrm{wet}}$ the hydraulic diameter, which is defined based on the cross-sectional area of the fluid flow A_{fluid} and the wetted perimeter of this cross-section P_{wet} [35]. The calculated Reynolds number is approximately 2199 at a flow rate of 10 L/h, given a water density and viscosity of 997 kg/m³ and 0.7978 mPa s at 30 °C, respectively, and a hydraulic diameter of 2 mm for the flat sheet spiral. This puts the flow in the transitional regime. Turbulent flow does occur, however, in the bends of the inlet and outlet pipe as can be seen in Figure 2. Therefore, it was critical to use the “Turbulent Flow” physics. This approach contrasts with the literature, where laminar flow is typically assumed in the studied modules, which are generally hollow fibre modules [36–39]. Magalhães et al. [40] highlighted the positive effects of turbulence, demonstrating that increased turbulence levels can reduce the thickness of the polarization layer. However, higher pumping velocities and turbulence also result in a greater pressure drop across the membrane. If the transmembrane pressure exceeds a critical threshold, it can result in a substantial loss of the liquid membrane phase [41].

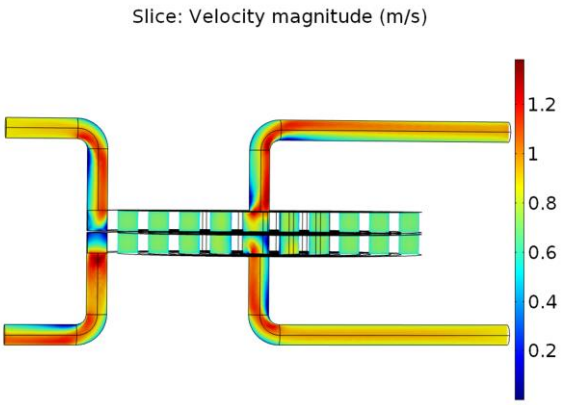

Figure 2. Velocity profile in the flat sheet module at a flow rate of 10 L/h, generated in COMSOL Multiphysics 5.1.

The effect of the mode of operation – co-current vs. counter-current – was simulated by exchanging the strip side "Inlet" and "Inflow" boundaries with their respective "Outlet" and "Outflow" boundaries. In the simulations, three pseudo-compounds were defined as solutes in the feed solution with pKa values of 9.4, 10.0, and 10.6. The simulations show that the mode of operation has a negligible effect on both the flux and the extraction (< 1.3% variation). Convection was assumed to be the dominating transport mechanism within the buffer phases [42]. This assumption was confirmed by varying the diffusion coefficients of all compounds in the buffer phases between 10^{-10} and 10^{-8} m^2/s, which gave a relative variation of approximately -0.1 % for all fluxes (see Figure S4).

Since the support material influences the SLM extraction behaviour, the effect of the membrane properties – specifically the porosity, permeability, and diffusivity – on the extraction behaviour were studied as well. Membrane porosity plays a key role in extraction, as a more porous membrane enhances mass transfer through the SLM [31]. This is evident from the simulations, where increased porosity significantly improved extraction performance and solute flux (see Figure S5). Similarly, Hemmati et al. [43] reported that increasing the porosity-to-tortuosity ratio improved extraction performance. This result is consistent with the understanding that higher porosity and reduced tortuosity lower the mass transfer resistance of the porous membrane, thereby facilitating solute transport. In contrast to the buffer phases, where convection is the primary transport mechanism, diffusion is assumed to dominate mass transfer in the liquid membrane (LM) phase. To verify this, the effect of the membrane

permeability and diffusivity were analysed. Membrane permeability, which affects convection through the membrane, was initially estimated at 0.06326 D, similar to that of a PVDF/MAF-4 membrane [44]. However, because the permeability depends on the transmembrane pressure (TMP) – which should be minimised to avoid extractant loss – its impact was found to be negligible, with variations by a factor 10^2 and 10^{-2} causing only minor deviations (~ 10^{-5}%) in extraction and flux (see Figure S6). On the other hand, solute diffusivity, which directly affects diffusion in the LM phase, showed a stronger influence. When diffusivity values were varied between 10^{-10} and 10^{-8} m²/s (see Figure S7), a linear correlation with extraction efficiency and flux was observed on a log-log scale. This confirms that diffusion is the dominant transport mechanism within the LM phase.

3.2 CFD model building and validation

To complement the simulations, an experimental study was performed to study the effects of the process conditions – specifically, flow rate, feed concentration, and pH – on process performance. The effective diffusion coefficients of the amines in the liquid membrane phase were calculated using COSMO-RS (see Figure S8). At T = 30 °C, the effective diffusivities of MBA, MPPA, and IPA are equal to $1.57 \cdot 10^{-10}$, $1.35 \cdot 10^{-10}$, and $2.06 \cdot 10^{-10}$ m²/s, respectively. The molecular volumes of MBA, MPPA, and IPA equal 170.17, 215.81, and 97.2 Å^3, respectively, which indicates that larger molecular volumes result in slower diffusion rates. As the COMSOL model does not account for amine partitioning, which occurs at the feed-membrane interphase, the COMSOL diffusivity D_{COMSOL} was treated as the product of the effective diffusivity D_{eff} and the amine-specific partition coefficient K_{p}^{i}:

$$D_{\mathrm{COMSOL}} = D_{\mathrm{eff}} \cdot K_{\mathrm{p}}^{i} \tag{5}$$

In order to determine the partition coefficient of each amine, the COMSOL diffusivities were first fitted to the model at the standard conditions, as specified in Table 1. This resulted in the COMSOL diffusivities ($D_{\mathrm{COMSOL}}^{\mathrm{fitted}}$) and the partition coefficients (K_{p}^{i}) for MBA, MPPA, and IPA, as specified in Table 2. The much higher partition coefficient of MPPA could be linked with its higher hydrophobicity, which is indicated by its higher logP value. The same is valid for the hydrophilic IPA molecule, as its K_{p}^{i} is much lower

in comparison with MPPA. Interestingly, the MBA partition coefficient is similar to the one of IPA, despite their difference in hydrophobicity. Nonetheless, the fitted COMSOL diffusivities for MBA, MPPA, and IPA at the standard conditions were used for the other CFD simulations.

Table 2. The effective diffusivity, the fitted COMSOL diffusivity, the partition coefficient, and the XLogP3 values for the considered amines. The XLogP3 values were retrieved from Kim et al. [45].

Solute	D_{eff}	$D_{\mathrm{COMSOL}}^{\mathrm{fitted}}$	K_{p}^{i}	XLogP3
	m²/s	m²/s	-	-
MBA	$1.57 \cdot 10^{-10}$	$2.39 \cdot 10^{-10}$	1.52	1.2
MPPA	$1.35 \cdot 10^{-10}$	$7.28 \cdot 10^{-10}$	5.39	2
IPA	$2.06 \cdot 10^{-10}$	$2.29 \cdot 10^{-10}$	1.11	0.1

The validation of the CFD model was carried out by comparing simulated solute flux and recovery values with experimental measurements across all the tested conditions, including flow rates, feed concentrations, and feed pH levels. The scatter plots in Figure 3 (a) and (b) show the simulated flux and recovery data on the *y*-axis versus the experimental values on the *x*-axis, respectively, with each point representing a different experimental condition. The data points are scattered around the 45-degree line (dashed line), which represents perfect agreement between simulated and experimental values. Points that are closer to this line indicate better alignment between model predictions and experimental results. For solute fluxes below approximately 5 g/(m²h) and recoveries below 40%, most points lie near the line, indicating good agreement. However, at higher flux values, particularly those exceeding 10 g/(m²h), there is a noticeable deviation, especially for variations in feed pH (blue points), where simulated values tend to be lower than the experimental data. This discrepancy is also clear from the RMSE values of the solute fluxes and recoveries (refer to Table S8), which show higher values at elevated pH levels. The following sections provide a more detailed analysis of the various effects.

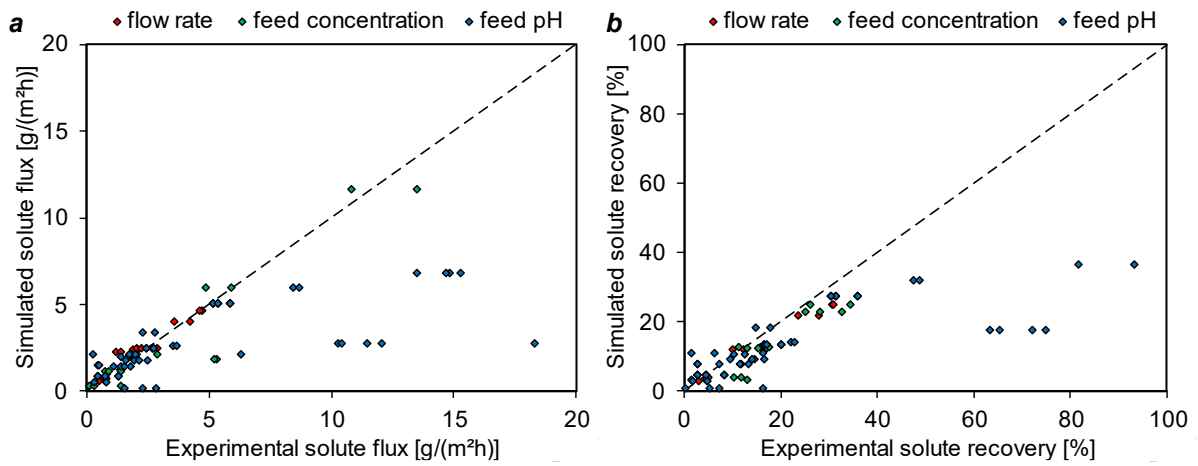

Figure 3. Comparison of the simulated and experimental solute fluxes and recovery.

3.3 Effect of process conditions

The velocity in the buffer phases was varied by adapting the “Inlet” boundary conditions in the “Turbulent Flow” physics, with flow rates ranging from 5 to 10 L/h. A maximum flow rate of 10 L/h was applied to prevent a transmembrane pressure (TMP), which could lead to membrane failure due to solvent loss from the membrane pores. As shown in Figure 4, the solute fluxes and recoveries remain nearly constant for variations of the flow rates. No significant difference is observed compared to the standard conditions (10 L/h), except for a notable decrease in the MBA flux and recovery at 5 L/h. This decrease at lower flow rates could be attributed to the lower pH values during the experimental tests, *i.e.*, the feed buffer had a pH of 10.00, 10.15, and 10.27 for the experiments at a flow rate of 5, 7.5, and 10 L/h. After pH correction, the model shows good alignment with the experimental results, achieving RMSE values of 0.43 and 3.91 for the solute flux and recovery, respectively.

The literature typically reports a decrease in the solute recovery at higher flow rates due to reduced residence time in the module [39,46,47]. However, most reported experiments are conducted over shorter runtimes, while longer runtimes may show that higher flow rates can lead to similar or even improved recoveries due to increased solute flux and recirculation effects. In this study, the simulated MBA recovery was found to be 0.0272 and 0.0152% at flow rates of 5 and 10 L/h, respectively, for a single run-through. The residence time during a single pass through the module was approximately 0.404 s at a flow rate of 10 L/h, indicating that only a small fraction of

MBA can be extracted during each pass. However, after 24 hours, the MBA recoveries were 12.06 and 13.30% at flow rates of 5 and 10 L/h, respectively, highlighting the effect of runtime.

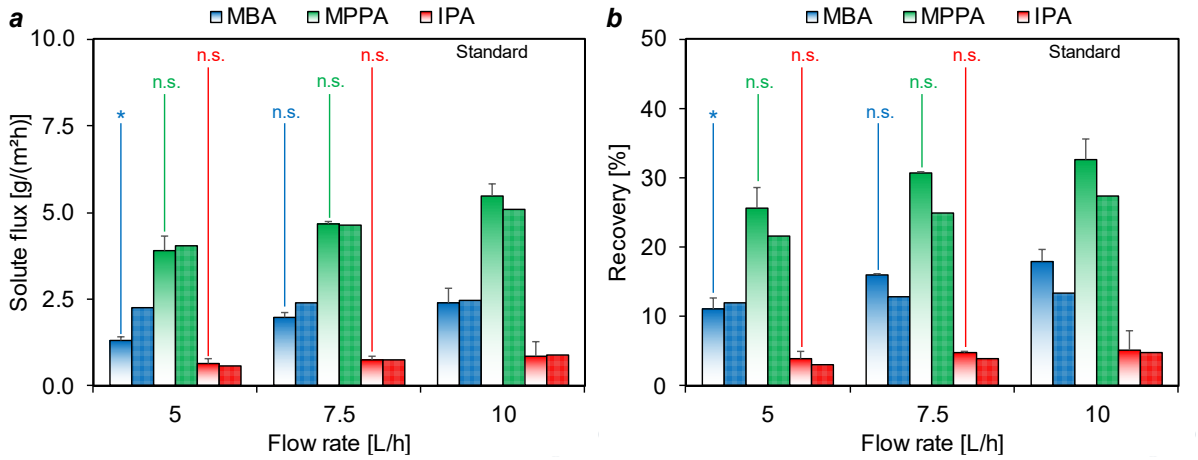

*Figure 4. Effect of the feed and strip flow rates on (a) the solute flux, and (b) the solute recovery of the amines, compared with experimental data. * indicates a significant difference ($p < 0.05$) with the standard conditions, while n.s. indicates no significant difference ($p > 0.05$). Refer to Table S9 for the complete statistical analysis.*

To study the effect of the feed concentration, the inflow and initial conditions of the amine concentrations were adjusted in the "Transport of Diluted Species in Porous Media" physics. The results for the considered concentrations with respect to the solute fluxes and recoveries are given in Figure 5 (a) and (b), respectively. In contrast to variations in the flow rate, a changing feed concentration results in a nearly constant recovery, but an increased flux for higher concentrations, which is consistent with the higher driving force [48]. As the concentration gradient of the unprotonated amines, which is the driving force for diffusion through the SLM, increases, a similar recovery can be achieved across all the considered feed concentrations. As this recovery remains constant at higher concentrations, it follows that the flux will increase proportionally to the concentration. Again, the simulations align well with the experimental data with RMSE values of 1.15 and 5.22 for the solute flux and recovery, respectively. The actual pH varied slightly with different amine concentrations, *i.e.*, the feed buffer had pH values of 10.05, 10.27, and 10.15 for feed concentrations of 0.5, 1, and 2.5 g/L, respectively.

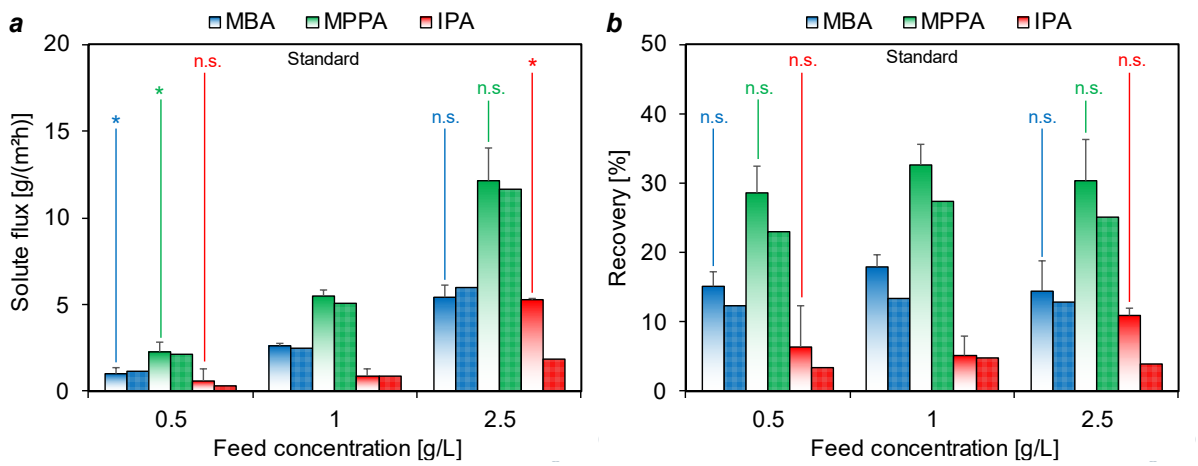

*Figure 5. Effect of the feed concentration on (a) the solute flux, and (b) the solute recovery of the amines, compared with experimental data. * indicates a significant difference ($p < 0.05$) with the standard conditions, while n.s. indicates no significant difference ($p > 0.05$). Refer to Table S10 for the complete statistical analysis.*

3.4 Effect of pH conditions and protonation kinetics

The process performance also depends on the pH conditions, as they affect the amine equilibrium. Specifically, the equilibrium in the buffer solutions shifts with pH, determining whether the amines are present in their unprotonated forms (MBA, MPPA, IPA) or protonated forms (MBAH+, MPPAH+, IPAH+). This protonation reaction is governed by an equilibrium constant related to the pKa values of the amines (see Section S3.2.2). For the amines, the following equilibrium reaction occurs between the protonated and deprotonated forms of the amines in alkaline media:

$$\mathrm{RNH_3^+ + OH^- \rightleftharpoons RNH_2 + H_2O} \quad (6)$$

Due to the elevated pH, the equilibrium of the previous reaction is shifted towards the right, *i.e.*, the protonated amine $\mathrm{RNH_3^+}$ is transformed to the deprotonated form $\mathrm{RNH_2}$. As charged molecules are not able to pass the ionic liquid phase due to repulsion with the charged cations and anions, only the uncharged, unprotonated amine is able to pass through to the strip side, where protonation occurs:

$$\mathrm{RNH_2 + H_3O^+ \rightleftharpoons RNH_3^+ + H_2O} \quad (7)$$

An acidic pH is required on the strip side to allow for a fast protonation, preventing back extraction. The effect of the kinetics of the protonation reaction occurring at the strip side was also investigated. The hypothetical scenarios of infinitely fast,

intermediate, and infinitely slow protonation kinetics were examined, corresponding to 100, 50, and 0% protonation, respectively. For all the scenarios, a strip concentration of 0.2 g/L was assumed, which is similar to the final amine concentration on the strip side at the end of a 24-hour experiment.

Assuming infinitely fast protonation kinetics, no significant change in extraction behaviour or fluxes was observed when the strip concentration increased from 0 to 0.2 g/L (refer to Figure S9). On the other hand, if the protonation kinetics are infinitely slow, the extraction and fluxes decreased significantly by 25, 38, and 90% for a pKa value of 9.4, 10.0, and 10.6, respectively, compared to when protonation kinetics are infinitely fast (refer to Figure S10). This large deviation for the different pKa values can be explained by comparing the concentration difference of unprotonated amines over the SLM, as presented in Table 3. At a pH of 10 and a feed concentration of 1 g/L, approximately 0.82 g/L of the solute with a pKa of 9.4 is deprotonated at the feed side, giving a gradient of the deprotonated amines of 0.62 g/L over the SLM. The drop in concentration compares closely to the simulated 25% drop in the flux. Similar conclusions can be drawn for solutes with a pKa of 10.0 and 10.6 (see Table 3).

Table 3. The concentration of protonated (C_{aH+}^{f}) and unprotonated (C_{a}^{f}) amines of varying pKa for a feed buffer at pH 10 and a feed concentration of 1 g/L. The strip is assumed to have a total amine concentration of 0.20 g/L without protonation.

pKa	$C_{\mathrm{a}}^{\mathrm{f}}$	$C_{\mathrm{aH+}}^{\mathrm{f}}$	$C_{\mathrm{a}}^{\mathrm{s}}$	$C_{\mathrm{aH+}}^{\mathrm{s}}$	$\Delta C_{\mathrm{a}}^{\mathrm{f-s}}$	Concentration decrease
-	g/L	g/L	g/L	g/L	g/L	%
9.4	0.82	0.18	0.2	0	0.62	24
10.0	0.52	0.48	0.2	0	0.32	38
10.6	0.22	0.78	0.2	0	0.02	91

The pH value of the strip buffer gives a negligible relative difference when varied between 2 and 4, compared with the standard simulation (see Figure S11). In contrast, the feed side pH had the largest influence on the extraction behaviour. Figure 6 reveals a clear trend; both the solute flux and recovery increase significantly at higher feed pH values, particularly at a pH of 11. A similar strong pH effect was observed for the extraction of vanillin by Cao et al. [39]. Interestingly, the simulations could not explain

the strong surge in the amine fluxes for a pH increase from 10.5 to 11. The RMSE values for the solute flux and recovery were 5.16 and 20.32, respectively. Note that the actual pH values of the prepared buffer solutions were 9.40, 9.83, 10.27, 10.68, and 11.10, respectively. This discrepancy may be due to the addition of amines, which raises the theoretical buffer pH.

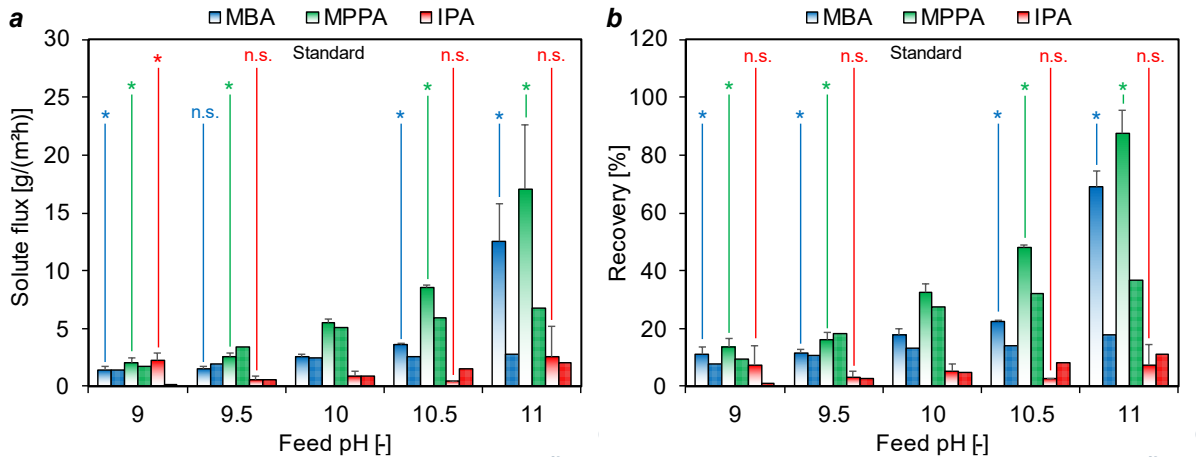

*Figure 6. Effect of the feed pH on (a) the solute flux, and (b) the solute recovery of the amines, compared with experimental data. * indicates a significant difference ($p < 0.05$) with the standard conditions, while n.s. indicates no significant difference ($p > 0.05$). Refer to Table S11 for the complete statistical analysis.*

However, based on the pKa values of the amines (see Table S3), the deprotonation degree of MBA increases by less than 5% for an increase in the pH from 10.5 to 11.0 (see Table 4), which could not explain the surge in the flux by a factor of three. Similar observations could be made for MPPA and IPA. Based on these observations, a new mass transfer mechanism must be proposed.

Table 4. Deprotonation degrees (x_i) and experimental fluxes (J_i^{exp}) of the amines at various pH levels.

pH	x_{MBA}	$J_{\mathrm{MBA}}^{\mathrm{exp}}$	x_{MPPA}	$J_{\mathrm{MPPA}}^{\mathrm{exp}}$	x_{IPA}	$J_{\mathrm{IPA}}^{\mathrm{exp}}$
-	%	g/(m²h)	%	g/(m²h)	%	g/(m²h)
9.0	28.5	1.45	9.7	2.04	1.4	2.22
9.5	55.7	1.54	24.2	2.55	7.4	0.56
10.0	79.9	2.62	50.0	5.47	21.6	0.84
10.5	92.6	3.60	75.4	8.56	44.7	0.48
11.0	97.5	10.72	90.1	14.34	70.2	2.57

3.5 Proposed mass transfer mechanism

As presented in Figure 6, an increase in the pH from 10.5 to 11.0 significantly enhances the solute fluxes and recoveries through the SLM. This could only be linked to the higher hydroxide concentration in the feed solution. To understand this pH dependence, the membrane structure itself should be considered, and more specifically, the interphase between the ionic liquid inside the membrane and the feed phase. Ionic liquids exhibit a dense structuring of their constituent ions at solid and fluid interphases due to strong cohesive interactions, namely Coulombic, van der Waals, and hydrogen bonding [49].

The ions of long-chained ionic liquids can organise themselves in three ways. First, the ions may form a thin, electroneutral layer of cations and anions that are oriented parallel to the substrate. This type of structure can be observed in apolar and hydrophobic substrates, having favourable interactions with hydrocarbon contaminants. Second, the ions may form a first layer in which most alkyl chains are oriented perpendicularly to the surface. Consequently, regions of bilayers appear on the substrate. This structure can be found on more hydrophilic substrates, such as SiO_2 and wet MoS_2. Third, a multiple bilayer structure could be formed, with all alkyl chains oriented perpendicularly to the substrate in the first layer. A further organisation into apolar and polar domains (with increasing disorder in each layer) can propagate towards the bulk of the ionic liquid. This final structure is found mostly on highly charged surfaces, either positive or negative [49].

The discussed structures are only suited for long-chained imidazolium ionic liquids. On the other hand, long-chained phosphonium cations, such as $[P_{6,6,6,14}]^+$, show no multilayer behaviour or stratification but a gradual displacement of the ions without the formation of distinct layers. Radiom et al. [50] linked this phenomenon to the large size, flexibility, and highly delocalised charge of the cation. Like Bou Tannous et al. [49], they also observed that the presence of a strong charge on the substrate surface led to a considerably higher layer thickness with more cations. Cooper et al. [51] also found that $[P_{6,6,6,14}]^+$ cations can adsorb on slightly negatively charged surfaces, leading to a cation-rich boundary layer.

In this work, a hydrophobic PTFE membrane was used for the extraction testing. According to Barišić et al. [52], PTFE shows a negative surface charge at a pH above ± 3, which indicates that hydroxide ions can accumulate more easily in the electrical interfacial layer (EIL) than hydronium ions, *i.e.*, hydroxide ions enter the boundary layer and simultaneously push out hydronium ions towards the bulk of the solution. This process occurs spontaneously. For an increase of the pH from 10.5 to 11.0, the hydroxide concentration increases from 0.316 to 1 mM, representing a threefold increase. Due to this higher concentration, more hydroxide ions can enter the EIL of the PTFE membrane leading to a stronger negative charge on the surface. As stated by Cooper et al. [51], $[P_{6,6,6,14}]^+$ cations show a surfactant-like structure, which could lead to high surface activity and strong adsorption, especially on negatively charged surfaces. Furthermore, the bulkiness of the $[P_{6,6,6,14}]^+$ cation prevents the incorporation of anions into the boundary layer. Thus, a cation-rich boundary layer is created close to the membrane-feed interphase. Additionally, by increasing the bulk water content of the ionic liquid (which is 2.22 wt% if fully saturated [14]), the interfacial structure can transform into a more heterogeneous structure. This effect can be attributed to a water-enhanced segregation of the long-chained ionic liquid into polar and apolar nanodomains.

Therefore, the proposed mass transfer mechanism, which is presented schematically in Figure 7, can be summarised as follows. First, hydroxide ions in the feed phase accumulate at the boundary layer of the PTFE membrane and displace hydronium ions. The higher OH^- concentration leads to a stronger negative surface charge of the PTFE membrane. The negatively charged membrane surface promotes the adsorption of $[P_{6,6,6,14}]^+$ cations near the membrane-feed interphase. Then, a boundary layer rich in cations forms close to the interphase. The cation-rich boundary layer enhances the partitioning of amine solutes between the feed phase and the liquid membrane phase. Additional segregation into polar and apolar nanodomains may occur, due to water absorption by the ionic liquid.

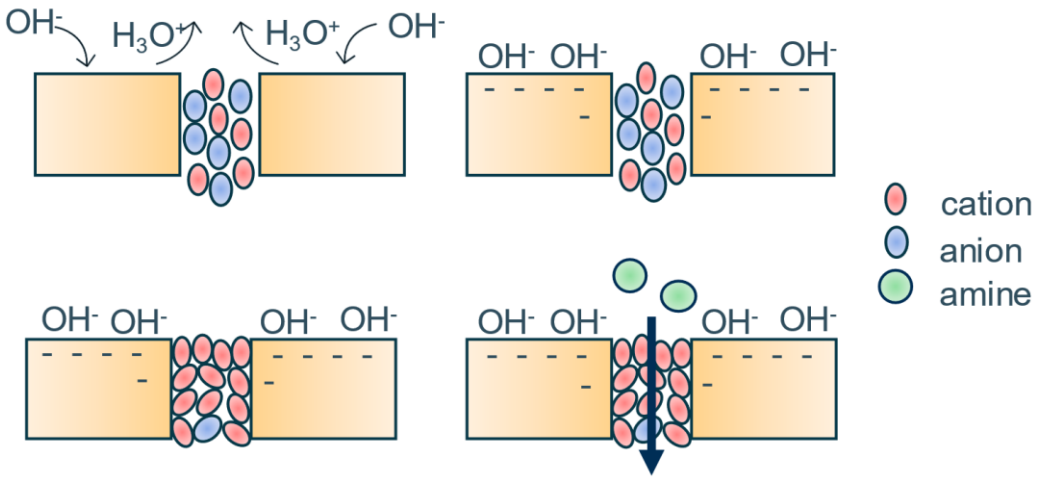

Figure 7. Schematic diagram of the proposed mass transfer mechanism.

4 Conclusion

The objective of this work was to experimentally investigate the separation of the aromatic amines α-methylbenzylamine (MBA) and 1-methyl-3-phenylpropylamine (MPPA) from isopropyl amine (IPA) in an alkaline feed buffer. The separation process was carried out using the ionic liquid $[P_{6,6,6,14}][N(Tf)_2]$ as the extractant in a flat sheet supported liquid membrane (SLM) setup operated in recycle mode. The experimental tests showed that a linear flux increase was observed for higher feed concentrations, which is due to the higher driving force between the feed and strip phase. While flow velocity had minimal impact, a higher pH of the feed buffer strongly affected both solute fluxes and recoveries.

To complement the experimental data, computational fluid dynamics (CFD) simulations were performed to elucidate the underlying physical phenomena. Varying the flow velocity had limited impact on extraction behaviour, while the feed solute concentration exhibited a linear relationship with flux, consistent with experimental findings. The kinetics of protonation also played a critical role, with infinitely fast protonation kinetics resulting in the highest extraction rates, attributed to a stronger driving force for mass transfer. However, the CFD simulations did not reveal a strong pH effect on extraction, as observed experimentally. Within the simulations, the pH only influences the amine equilibrium, which alone could not account for the experimentally observed surge in the fluxes.

The discrepancy between experimental and simulated pH effects points to a novel mass transfer mechanism in which elevated hydroxide concentrations likely induce a charged membrane surface, attracting ionic liquid cations close to the interphase and enhancing amine partitioning into the ionic liquid phase, explaining the improved extraction performance at higher pH values. This insight offers a deeper understanding of the role of pH in the system, underscoring the complexity of interactions at the membrane interface and suggesting avenues for optimizing membrane-based separations in similar applications.

Acknowledgement

The authors would like to thank the support of the Flemish Strategic Basic Research Program of the Catalisti cluster and Flanders Innovation & Entrepreneurship in the framework of the EASiCHEM project (contracts HBC.2018.0484 and K200522N). The authors also acknowledge the support provided by the Scientific and Technological Research Council of Turkey (TUBITAK)-2219 for granting the International Postdoctoral Research Fellowship Program to Nilay Baylan. Additionally, the authors would like to thank Emma Lodewijckx and Sean Van Gestel for the excellent work they performed in establishing a working CFD simulation.

Conflict of interest statement

The authors declare that there is no conflict of interest.

Declaration of generative AI and AI-assisted technologies in the writing process

During the preparation of this work the authors used ChatGPT in order to enhance the clarity, coherence, and overall quality of the manuscript. After using this tool/service, the authors reviewed and edited the content as needed and takes full responsibility for the content of the publication.

References

[1] F. Mutti, Molecular science: The importance of sustainable manufacturing of chiral amines, (2020).

[2] D. Ghislieri, A.P. Green, M. Pontini, S.C. Willies, I. Rowles, A. Frank, G. Grogan, N.J. Turner, Engineering an enantioselective amine oxidase for the synthesis of pharmaceutical building blocks and alkaloid natural products, J Am Chem Soc, 135 (2013) 10863–10869.

[3] G. Rehn, P. Adlercreutz, C. Grey, Supported liquid membrane as a novel tool for driving the equilibrium of ω-transaminase catalyzed asymmetric synthesis, J Biotechnol, 179 (2014) 50–55.

[4] D. Koszelewski, K. Tauber, K. Faber, W. Kroutil, ω-Transaminases for the synthesis of non-racemic α-chiral primary amines, Trends Biotechnol, 28 (2010) 324–332.

[5] P. Tufvesson, J. Lima-Ramos, J.S. Jensen, N. Al-Haque, W. Neto, J.M. Woodley, Process considerations for the asymmetric synthesis of chiral amines using transaminases, Biotechnol Bioeng, 108 (2011) 1479–1493.

[6] C. Amabile, T. Abate, S. Chianese, D. Musmarra, R. Muñoz, Exploring 1,3-dioxolane extraction of poly(3-hydroxybutyrate) and poly(3-hydroxybutyrate-co-3-hydroxyvalerate) from Methylocystis hirsuta and mixed methanotrophic strain: Effect of biomass-to-solvent ratio and extraction time, Polymers (Basel), 16 (2024).

[7] J. Grau, C. Azorín, J.L. Benedé, A. Chisvert, A. Salvador, Use of green alternative solvents in dispersive liquid-liquid microextraction: A review, J Sep Sci, 45 (2022) 210–222.

[8] G. Van Eygen, B. Van der Bruggen, A. Buekenhoudt, P. Luis Alconero, Efficient membrane-based affinity separations for chemical applications: A review, Chemical Engineering and Processing - Process Intensification, 169 (2021) 108613.

[9] G. Van Eygen, B. Van der Bruggen, A. Buekenhoudt, P. Luis Alconero, Efficient membrane-based affinity separations for chemical applications: A review, Chemical Engineering and Processing - Process Intensification, 169 (2021).

[10] A. Gabelman, S.T. Hwang, Hollow fiber membrane contactors, J Memb Sci, (1999).

[11] P.K. Parhi, Supported liquid membrane principle and its practices: A short review, J Chem, 2013 (2013).

[12] G. Rehn, B. Ayres, P. Adlercreutz, C. Grey, An improved process for biocatalytic asymmetric amine synthesis by in situ product removal using a supported liquid membrane, J Mol Catal B Enzym, 123 (2016) 1–7.

[13] G. Van Eygen, C. Echezuria, A. Buekenhoudt, João.A.P. Coutinho, B. Van der Bruggen, P. Luis, COSMO-RS screening of organic mixtures for membrane extraction of aromatic amines: TOPO-based mixtures as promising solvents, Green Chemical Engineering, (2024).

[14] G. Van Eygen, D. Mariën, A. Vananroye, C. Clasen, B. Van der Bruggen, A. Buekenhoudt, J.A.P. Coutinho, P. Luis, Facilitated solvent screening for membrane-based extraction of chiral amines via a priori simulations, J Mol Liq, 375 (2023) 121351.

[15] R. Craveiro, L.A. Neves, A.R.C. Duarte, A. Paiva, Supported liquid membranes based on deep eutectic solvents for gas separation processes, Sep Purif Technol, 254 (2021) 117593.

[16] M. Ishaq, M.A. Gilani, Z.M. Afzal, M.R. Bilad, A.S. Nizami, M. Rehan, E. Tahir, A.L. Khan, Novel poly deep eutectic solvents based supported liquid membranes for CO2 capture, Front Energy Res, 8 (2020).

[17] E. Zurob, E. Quijada-Maldonado, R. Castro-Muñoz, J. Romero, A. Plaza, R. Cabezas, Development of an asymmetric cellulose acetate-ionic liquid P6,6,6,14[PHOS] gel membrane for the perstraction of succinic acid from a

model fermentation solution of yarrovia lipolytica, Sep Purif Technol, 354 (2025) 129199.

[18] G. Rehn, P. Adlercreutz, C. Grey, Supported liquid membrane as a novel tool for driving the equilibrium of ω-transaminase catalyzed asymmetric synthesis, J Biotechnol, 179 (2014) 50–55.

[19] G. Rehn, P. Adlercreutz, C. Grey, Supported liquid membrane as a novel tool for driving the equilibrium of ω-transaminase catalyzed asymmetric synthesis, J Biotechnol, 179 (2014) 50–55.

[20] V. Udoewa, V. Kumar, Computational Fluid Dynamics, in: Applied Computational Fluid Dynamics, 2012.

[21] J. Tu, G.H. Yeoh, C. Liu, Computational fluid dynamics: a practical approach, Butterworth-Heinemann, 2018.

[22] J. Blazek, Computational fluid dynamics: principles and applications, Butterworth-Heinemann, 2015.

[23] J.F. Wendt, Computational fluid dynamics: an introduction, Springer Science & Business Media, 2008.

[24] C.-L. Lin, M.H. Tawhai, G. McLennan, E.A. Hoffman, Computational Fluid Dynamics Computational Fluid Dynamics CSE-801, IEEE Engineering in Medicine and Biology Magazine, 28 (2009) 25–33.

[25] M. Ghadiri, M. Ghasemi Darehnaei, S. Sabbaghian, S. Shirazian, Computational simulation for transport of priority organic pollutants through nanoporous membranes, Chem Eng Technol, 36 (2013) 507–512.

[26] M. Hemmati, N. Nazari, A. Hemmati, S. Shirazian, Phenol removal from wastewater by means of nanoporous membrane contactors, Journal of Industrial and Engineering Chemistry, 21 (2015) 1410–1416.

[27] M. Ghadiri, S. Shirazian, Computational simulation of mass transfer in extraction of alkali metals by means of nanoporous membrane extractors, Chemical Engineering and Processing: Process Intensification, 69 (2013) 57–62.

[28] A. Muhammad, M. Younas, M. Rezakazemi, CFD simulation of copper(II) extraction with TFA in non-dispersive hollow fiber membrane contactors, Environmental Science and Pollution Research, 25 (2018) 12053–12063.

[29] Y. Cao, A. Khan, S. Sarkar, A.B. Albadarin, Extraction of penicillin G from aqueous solution using a membrane contactor: Numerical investigation, Arabian Journal of Chemistry, 14 (2021) 103230.

[30] A. Qatezadeh Deriss, S. Langari, M. Taherian, Computational fluid dynamics modeling of ibuprofen removal using a hollow fiber membrane contactor, Environ Prog Sustain Energy, (2021).

[31] G. Van Eygen, S. Keuppens, X. De Breuck, B. Swankaert, P. Boura, E. Loccufier, J. Kosek, D. Ramasamy, F. Nahra, A. Buekenhoudt, K. De Clerck, B. Van der Bruggen, P. Luis, Comparison of distinctive polymeric membrane structures as support materials for membrane extraction of chiral amines, Sep Purif Technol, 352 (2025).

[32] H.W. Khan, A.V.B. Reddy, M.M.E. Nasef, M.A. Bustam, M. Goto, M. Moniruzzaman, Screening of ionic liquids for the extraction of biologically active compounds using emulsion liquid membrane: COSMO-RS prediction and experiments, J Mol Liq, (2020).

[33] Z. Zhang, R. Lu, Q. Zhang, J. Chen, W. Li, COSMO-RS based ionic liquid screening for the separation of acetonitrile and ethanol azeotropic mixture, Journal of Chemical Technology and Biotechnology, (2020).

[34] J.P. Wojeicchowski, C. Marques, L. Igarashi-Mafra, J.A.P. Coutinho, M.R. Mafra, Extraction of phenolic compounds from rosemary using choline chloride–based deep eutectic solvents, Sep Purif Technol, (2021).

[35] D.K. Puckert, U. Rist, Experiments on critical Reynolds number and global instability in roughness-induced laminar-turbulent transition, J Fluid Mech, 844 (2018) 878–904.

[36] M. Ghadiri, M. Ghasemi Darehnaei, S. Sabbaghian, S. Shirazian, Computational simulation for transport of priority organic pollutants through nanoporous membranes, Chem Eng Technol, 36 (2013) 507–512.

[37] A. Muhammad, M. Younas, M. Rezakazemi, CFD simulation of copper(II) extraction with TFA in non-dispersive hollow fiber membrane contactors, Environmental Science and Pollution Research, 25 (2018) 12053–12063.

[38] B. Swain, K.K. Singh, A.K. Pabby, Numerical simulation of uranium extraction from nitric acid medium using hollow-fiber contactor, Solvent Extraction and Ion Exchange, 37 (2019) 526–544.

[39] Y. Cao, M. Ghadiri, M. Rezakazemi, A. Marjani, M. Pishnamazi, S. Shirazian, Computational modelling of separation and purification of vanillin using microporous membranes, J Mol Liq, (2021).

[40] H.L.F. Magalhães, A.G.B. De Lima, S.R.D.F. Neto, H.G. Alves, J.S. De Souza, Produced water treatment by ceramic membrane: A numerical investigation by computational fluid dynamics, Advances in Mechanical Engineering, 9 (2017) 168781401668864.

[41] A.J.B. Kemperman, D. Bargeman, T. Van Den Boomgaard, H. Strathmann, Stability of supported liquid membranes: State of the art, Sep Sci Technol, (1996).

[42] Y. Cao, A. Khan, S. Sarkar, A.B. Albadarin, Extraction of penicillin G from aqueous solution using a membrane contactor: Numerical investigation, Arabian Journal of Chemistry, 14 (2021) 103230.

[43] M. Hemmati, N. Nazari, A. Hemmati, S. Shirazian, Phenol removal from wastewater by means of nanoporous membrane contactors, Journal of Industrial and Engineering Chemistry, 21 (2015) 1410–1416.

[44] R. Wu, Y. Tan, F. Meng, Y. Zhang, Y.X. Huang, PVDF/MAF-4 composite membrane for high flux and scaling-resistant membrane distillation, Desalination, 540 (2022) 116013.

[45] S. Kim, J. Chen, T. Cheng, A. Gindulyte, J. He, S. He, Q. Li, B.A. Shoemaker, P.A. Thiessen, B. Yu, L. Zaslavsky, J. Zhang, E.E. Bolton, PubChem 2023 update, Nucleic Acids Res., 51 (2023) D1373–D1380.

[46] A. Muhammad, M. Younas, M. Rezakazemi, Quasi-dynamic modeling of dispersion-free extraction of aroma compounds using hollow fiber membrane contactor, Chemical Engineering Research and Design, 127 (2017) 52–61.

[47] A. Muhammad, W. Ali, I. Ahmad, M. Younas, Performance evaluation of hollow fiber membrane contactors for dispersion-free extraction of Cu2+ through modelling and simulation, Periodica Polytechnica Chemical Engineering, 61 (2017) 133–143.

[48] M. Ghadiri, S.N. Ashrafizadeh, Mass transfer in molybdenum extraction from aqueous solutions using nanoporous membranes, Chem Eng Technol, 37 (2014) 597–604.

[49] L. Bou Tannous, M. Simoes Santos, Z. Gong, P.H. Haumesser, A. Benayad, A.A.H. Padua, A. Steinberger, Effect of Surface Chemistry on the Electrical Double Layer in a Long-Chain Ionic Liquid, Langmuir, 39 (2023) 16785–16796.

[50] M. Radiom, P. Pedraz, G. Pilkington, P. Rohlmann, S. Glavatskih, M.W. Rutland, Anomalous interfacial structuring of a non-halogenated ionic liquid: Effect of substrate and temperature, Colloids and Interfaces, 2 (2018) 1–14.

[51] P.K. Cooper, C.J. Wear, H. Li, R. Atkin, Ionic Liquid Lubrication of Stainless Steel: Friction is Inversely Correlated with Interfacial Liquid Nanostructure, ACS Sustain Chem Eng, 5 (2017) 11737–11743.

[52] A. Barišić, J. Lützenkirchen, G. Lefévre, T. Begović, The influence of temperature on the charging of polytetrafluoroethylene surfaces in electrolyte solutions, Colloids Surf A Physicochem Eng Asp, 579 (2019) 123616.